Investigation of Time–Frequency Features for GPR Landmine Discrimination

Timofey Grigorievich Savelyev, Luc van Kempen, Hichem Sahli, *Member, IEEE*, Juergen Sachs, and Motoyuki Sato, *Senior Member, IEEE*

***Abstract*—Ground-penetrating radar (GPR) is capable to detect plastic antipersonnel landmines as well as other subsurface targets. In order to reduce false alarms, an option of automatic landmine discrimination from neutral minelike targets would be very useful. This paper presents a possibility for such discrimination and analyzes it experimentally. The authors investigate time–frequency features of an ultrawideband (UWB) target response for the discrimination between buried landmines and other objects. The discrimination method includes the extraction of an early-time target impulse response, its time–frequency transformation, and the extraction of time–frequency features based on a singular value decomposition of the transformed image. In order to take into account the changes in the UWB target signals, the experimental conditions are completely controlled to focus on the behavior of the target's response with respect to its depth and the horizontal position of the GPR above it. The dependence of the features on the GPR bandwidth is analyzed as well. The Mahalanobis distance is used as a criterion for optimal discrimination. The obtained results define the best features and conditions when the landmine discrimination is successful. For comparison, the discriminant power of the proposed features has been tested on a dataset, acquired during a field campaign in Angola.**

***Index Terms*—Ground-penetrating radar (GPR), landmine discrimination, Mahalanobis distance, singular value decomposition (SVD), time–frequency features, ultrawideband (UWB), Wigner distribution (WD).**

I. Introduction

DEMINING of abandoned minefields is a serious problem for many countries. Its solution requires advanced technologies such as ultrawideband ground-penetrating radar (UWB GPR) that can detect a shallowly buried low-metal landmine [1]–[6]. The combination of an antenna array with synthetic aperture radar (SAR) technologies makes the detection possible even for inhomogeneous soil with a rough ground surface [1]–[3]. However, the main problem in landmine clearance is the false alarm rate reduction, i.e., how to discriminate, after detection, between a landmine and other objects, since any object with a sufficient dielectric contrast with soil can be imaged (detected).

Metallic debris can be discriminated by the fusion of GPR and metal detector data [7]–[9]. However, metal detectors have a difficulty with low-metal landmines. Another possibility for landmine discrimination deals with spatial signatures of detected targets which has been evaluated in [10] and [11].

In this paper, we focus on target discrimination using GPR data only. From the literature, it has been shown that a unique information can be extracted from a 1-D GPR target response (A-scan) [12], [13]. The target impulse response needs to be acquired above the center of a target and cleared from clutter. We define clutter as the reflection from the ground surface along with other unwanted reflections. Clutter can be removed using various modifications of the classic average subtraction for a flat ground surface or with an iterative parametric technique for a rough surface [13]–[15]. In GPR landmine detection, we deal mainly with the early-time target response, since the late-time terms are always distorted by multiple reflections between the target and the ground surface and by clutter residues. The early-time response may include reflections from the top and bottom of the target [12].

A possibility for straightforward landmine discrimination, based on inversion, has been investigated in [13]. The diameter, height, and dielectric constant of a target are estimated from a few-spike model of the target impulse response. To obtain such a model, the GPR impulse response must be deconvolved out of the data. For that, a model-based subset selection algorithm of deconvolution has been developed. This approach has been demonstrated for very dry soil that does not much influence the impulse responses of the target and the GPR itself. However, in the vicinity of the soil, the antenna impedance changes, making the GPR impulse response different from what is measured in an anechoic chamber. Besides, a moistened soil significantly attenuates high frequencies and thus changes the target's impulse response. Other deconvolution algorithms have been developed for GPR landmine discrimination as well [16], [17]. They are model independent and based on a regularization with automatic parameter estimation. Here, the physical difficulty to estimate accurately the soil influence on both GPR and target remains.

The proposed approach for target discrimination deals with the time–frequency analysis of the target's impulse response [17]–[27]. Such time–frequency signature can be treated as an

Manuscript received May 5, 2005; revised July 21, 2006. This work was supported in part by the Japan Science and Technology Corporation, the Japan Society for the Promotion of Science Grant-in-Aid for Scientific Research (S) 14102024 and (S) 18106008, and the Ministry of Education, Culture, Sports, Science and Technology (MEXT) Grant-in-Aid for Young Scientists (B) 16760324.

T. G. Savelyev is with the International Research Centre for Telecommunications and Radar, Delft University of Technology, 2628CD Delft, The Netherlands (e-mail: t.g.savelyev@irctr.tudelft.nl).

L. van Kempen and H. Sahli are with the Electronics and Informatics—ETRO, Vrije Universiteit Brussel, 1050 Brussels, Belgium (e-mail: lmkempen@etro.vub.ac.be; hsahli@etro.vub.ac.be).

J. Sachs is with the Department of Electrical Engineering and Information Technology, Technical University of Ilmenau, 98684 Ilmenau, Germany (e-mail: juergen.sachs@e-technik.tu-ilmenau.de).

M. Sato is with the Center for Northeast Asian Studies, Tohoku University, Sendai 980-8576, Japan (e-mail: sato@cneas.tohoku.ac.jp).

Digital Object Identifier 10.1109/TGRS.2006.885077

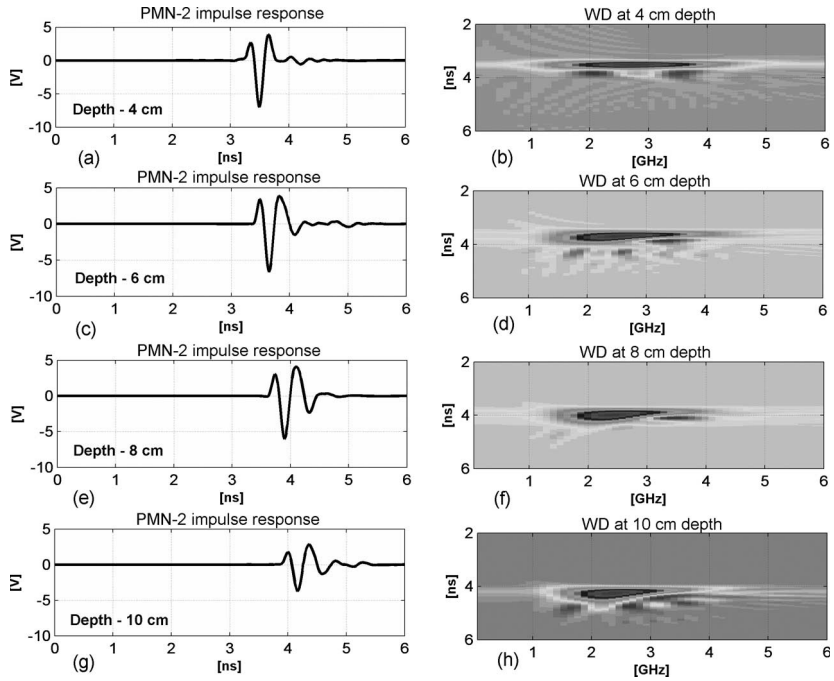

Fig. 1. Target impulse response and WD at different depths.

image which is easier to "recognize" than the corresponding 1-D time or frequency representation. The dielectric properties and the size of a target define the shape and intensity of the entire time–frequency image. In this paper, the Wigner distribution (WD) is used as a target signature due to its good properties [28].

Landmine discrimination based on the WD can be performed by singular value decomposition (SVD) and principal component analysis. Comparing singular values, due to their high sensitivity, provides discrimination between two even slightly different images. For GPR targets, the high frequencies become attenuated with depth, which changes the WD. Fig. 1 illustrates this effect for a model of the PMN-2 landmine buried in slightly wet sand with a moisture content of 8%. Such moisture was found to be typical in minefields of Afghanistan [8]. Therefore, the goal of this paper is to find robust SVD-based features of the nonstationary target response, allowing the discrimination of landmines from stones. We investigate the features' behavior for the same targets buried at different depths. The influence of the horizontal GPR offset from the target center is evaluated as well. The extracted features are used for cluster analysis based on the Mahalanobis distance [29], this has been done for various conditions.

In this paper, a dataset was acquired at the Tohoku University using a stepped-frequency GPR for a large frequency range. Reducing the data bandwidth made it possible to analyze the informative properties of low and high frequencies of target's responses and to find the optimal GPR bandwidth. In addition, a dataset acquired under realistic circumstances in Angola with a pseudonoise GPR was processed.

This paper is organized as follows. Section II describes the proposed time–frequency feature extraction algorithms. Feature clusters obtained by experiment are investigated in Section III, discussion and conclusions are given in Section IV.

II. Time–Frequency Feature Extraction

A. Extraction of Target Impulse Response

The first step in time–frequency feature extraction is the extraction of the target impulse response from a raw C-scan, acquired over a target. The C-scan is a three-dimensional GPR dataset obtained by sounding on a regular grid over an arbitrary rectangular surface. In our analysis, the data preprocessing consists of subtracting the antenna crosstalk, performing the inverse Fourier transform (IFT) for the stepped-frequency GPR, and removing the clutter. The antenna crosstalk represents a direct signal between the transmitting and the receiving antennas, which is commonly the strongest stationary component of the acquired data. As such, it can be acquired beforehand and then can be subtracted from every A-scan. If the GPR is stepped frequency, this can be done in the frequency domain directly. In this case, one should transform the data into the time domain using a fast algorithm of the IFT. Here, a symmetric window, such as Hanning, Kaiser, Chebyshev, and etc., can be applied to the frequency-domain data in order to avoid ringing in the time domain. One should take into account that such operation changes the shape of the signal and deteriorates the spatial resolution. If the GPR bandwidth is sufficiently large, it is preferable to apply a window with a wide flat top and smooth edges (a bandpass filter) to make sure that the acquired spectrum does not have sharp truncations.

The most difficult problem is removal of the ground reflection as the main part of clutter. In practice, the ground surface is usually rough which makes the clutter nonstationary. Since subtraction of the average A-scan is ineffective in this case, various techniques based on a moving window with alignment of the clutter estimate to each A-scan and subsequent subtraction are used. A common drawback of such techniques is a distortion of the target's response, especially for laid or flush

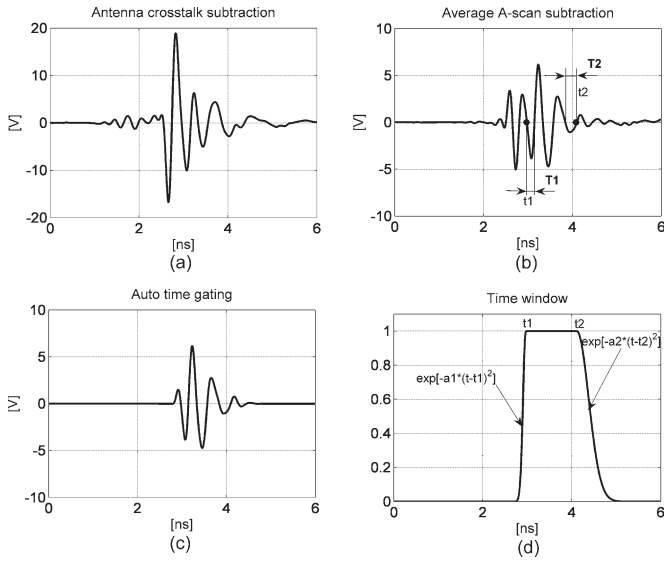

Fig. 2. Extraction of target impulse response from a raw A-scan.

targets. A promising solution has been proposed by van der Merwe and Gupta [14]. The idea is to represent the clutter with a number of the Prony parameters obtained with the total-least-squares approach. The parameters must be found iteratively to reconstruct the clutter in every A-scan and then to subtract it independently of other A-scans, which makes the technique robust against the surface roughness. Since this is not the focus of this paper, we employ here an ideal case of a flat ground surface with subsurface targets.

After clutter removal, a representative A-scan can be selected from the apex of the target hyperbola in a B-scan. A B-scan is a two-dimensional dataset obtained by sounding along a line. Since in practice it is often difficult to find the apex, we investigate the A-scans taken not only above the target's center but above the target's edges as well. In the selected A-scans, the early-time target response is considered as the strongest part of reflection. It is a distinct signal surrounded by clutter residues and followed by multiple reflections between the target and the ground surface. This signal needs to be extracted by time gating and then to be used for the time–frequency analysis.

For time gating, we developed an automatic algorithm based on two assumptions: 1) the strongest peak in A-scan after clutter removal belongs to the target and 2) the target impulse response represents a strong pulse of 2–3 short semiperiods followed by longer decaying semiperiods [12]. The latter is valid for UWB systems with nondispersive sensing signals. In case of dispersion, for example when spiral antennas are used, one needs to correct the acquired data with deconvolution. We assume that the strongest peak belongs to the second semiperiod of the target impulse response, and thus, we can use its position as a reference point. Starting from this point, it is easy to find the other semiperiods from zero crossings. Moving to the left from the reference point, we find the first semiperiod. To define the last semiperiod, we move to the right and apply an amplitude threshold for the peak values, specifically -10 dB with respect to the strongest peak. This process is illustrated in Fig. 2 which shows signals obtained consequently by antenna crosstalk subtraction, clutter removal, and time gating. The dots in Fig. 2(b) indicate the origin of the first target semiperiod (time instance t_1) and the end of the last semiperiod (time instance t_2), and also define the length of a gating window, more specifically its flat top.

In order to avoid signal truncation and to include the target information existing apart from the main semiperiods, the gating window should have smooth edges defined by a gaussoid as shown in Fig. 2(d). To suppress the strong clutter residues, we make the left edge sharper and determine α_1 from the duration of the first main semiperiod T_1 as $\exp\{-\alpha_1 T_1^2\} = 0.01$, i.e., $\alpha_1 = -\ln 0.01/T_1^2$. Then, the signal at the time instance $(t_1 - T_1)$ will be -40 dB lower than at the instance t_1. The parameter α_2 for the smoother and longer left edge can be computed from a condition $\exp\{-\alpha_2(3T_2)^2\} = 0.01$, where T_2 stands for the duration of the last main semiperiod, i.e., $\alpha_2 = -\ln 0.01/9T_2^2$. The parameters T_1 and T_2 can be found automatically from zero crossings. The signal after time gating is depicted in Fig. 2(c), while the gating window itself is shown in Fig. 2(d). Its flat part passes the early-time target impulse response without a distortion, and its edges smooth out the rest of the acquired data.

B. Time–Frequency Representation

The time–frequency transformation can be done with the Wigner transform, also well known as the Wigner-Ville transform (WD)

$$\mathrm{WD}(t,f) = \int_{-\infty}^{+\infty} s\left(t+\frac{\tau}{2}\right) s^*\left(t-\frac{\tau}{2}\right) \exp\{-j2\pi f\tau\}\, d\tau \tag{1}$$

where $s(t)$ is an analytic signal. This quadratic or bilinear transform provides a better time–frequency resolution compared to linear transforms such as the short-time Fourier transform, the continuous wavelet transform, or any other bilinear transform. The Wigner transform does not include any windowing or filtering, which can smear the signal properties, while many other transforms represent its smoothed versions. It does not require the selection of additional time–frequency functions or wavelets as it is based only on the signal to be transformed. Remarkable properties of the WD are independence of time, frequency, or phase shift and preservation of the signal energy. A serious drawback of the WD, namely cross terms for multiple signals, can be neglected for a single signal of the early-time target impulse response. Therefore, this distribution has been selected for our purpose.

Numerically the WD represents a large sparse real matrix where the target signal is concentrated inside a small dense submatrix. It is more efficient to deal with that submatrix only, which can be named as the effective WD (EWD) or time–frequency target image. Its borders can be determined in two ways. One approach is to set a certain threshold for the energy, say 99%, and then to extract the most compact area around the WD's maximum that contains the given energy. However, a discriminant target information represented by small image details can be removed as well. The second way is quasi-random and assumes a Gaussian distribution of the function $\mathrm{WD}^2(t,f)$

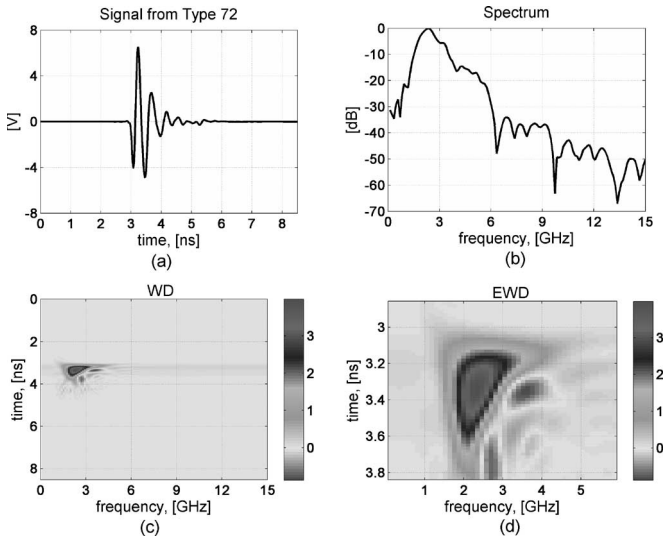

Fig. 3. Time–frequency representation of UWB GPR signal.

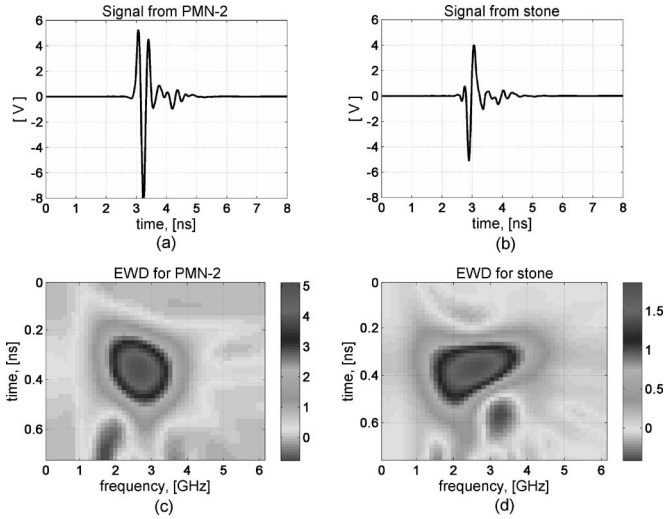

Fig. 4. Impulse response and EWD for a landmine and stone of similar size.

around the center of gravity of the WD. Then, we can determine the borders of the EWD with a statistical rule "$\pm 3\sigma$" using the center of gravity as a reference point. For a Gaussian distribution, 99.73% of its density is concentrated within the interval $[-3\sigma, 3\sigma]$ with respect to its mean. In this paper, we use the second technique to estimate the EWD.

The time and frequency coordinates of the center of gravity are given by

$$t_0 = \frac{1}{E} \int_0^{t_{\max}} \int_0^{f_{\max}} t \mathrm{WD}^2(t,f) df\, dt \tag{2}$$

$$f_0 = \frac{1}{E} \int_0^{f_{\max}} \int_0^{t_{\max}} f \mathrm{WD}^2(t,f) dt\, df \tag{3}$$

$$E = \int_0^{t_{\max}} \int_0^{f_{\max}} \mathrm{WD}^2(t,f) dt\, df. \tag{4}$$

The time and frequency variances are defined as follows:

$$\sigma_t^2 = \frac{1}{E} \int_0^{t_{\max}} \int_0^{f_{\max}} (t-t_0)^2 \mathrm{WD}^2(t,f) df\, dt \tag{5}$$

$$\sigma_f^2 = \frac{1}{E} \int_0^{f_{\max}} \int_0^{t_{\max}} (f-f_0)^2 \mathrm{WD}^2(t,f) dt\, df. \tag{6}$$

In (2)–(6), $t_{\max}$ is the maximal time of interest (e.g., the end of time window used for data acquisition) and $f_{\max}$ is the maximal frequency of interest (e.g., the highest acquired frequency).

Fig. 3 depicts a GPR signal of a Type 72 landmine, buried at a depth of 4 cm in moist sand, its spectrum, the WD, and EWD. In this particular case, the WD is a 512×128 matrix and the EWD is a submatrix of dimensions 59×50 that still contains 99% of the signal energy. The dimensions of the EWD, estimated automatically, represent the effective signal duration and bandwidth, which can differ for various targets and should be taken into account for feature extraction. Comparing Fig. 3(a) and (d), one can see that the EWD has the time duration of about 1 ns instead of 2.5 ns for the full signal. Thus, our discrimination technique uses only the strongest part of the target impulse response. This fits our algorithm of automatic time gating described in the previous section. Fig. 4 shows signals acquired for a PMN-2 landmine and a stone at a burial depth of 4 cm. In the time domain, the signals have different shape and amplitude but almost the same duration as shown in Fig. 4(a) and (b). The difference in shape results in the different EWDs or time–frequency images of the targets [Fig. 4(c) and (d)]. Note that the EWDs have negative values, which improves the discrimination between such images.

C. Principal Components of EWD

The singular components of the EWD matrix can be obtained by the SVD. We approximate the EWD with the first two singular triplets, which are the strongest, i.e., principal with respect to higher order components. The approximation is given by

$$\mathrm{EWD}_{K\times L} = \sum_{i=1}^{\min(K,L)} \sigma_i \mathbf{u}_i \mathbf{v}_i^{\mathrm{T}} \approx \sigma_1 \mathbf{u}_1 \mathbf{v}_1^{\mathrm{T}} + \sigma_2 \mathbf{u}_2 \mathbf{v}_2^{\mathrm{T}} \tag{7}$$

where σ_i is the ith singular value, $\mathbf{u}_i$ is the ith left singular vector of length K, $\mathbf{v}_i$ is the ith right singular vector of length L [30]. Decomposition (7) is illustrated in Fig. 5. If the columns of the EWD matrix stand for the time domain and the rows stand for the frequency domain, then $\mathbf{u}_i$ and $\mathbf{v}_i$ express time and frequency properties, respectively. Their matrix multiplication gives the shape of the ith singular component, while σ_i stands for the component's energy and defines its contribution to the original EWD matrix. The first singular component is the strongest, and it creates the high-energy part of the time–frequency image, i.e., the most robust part, as shown in Fig. 5(b). It can be interpreted as an image approximation,

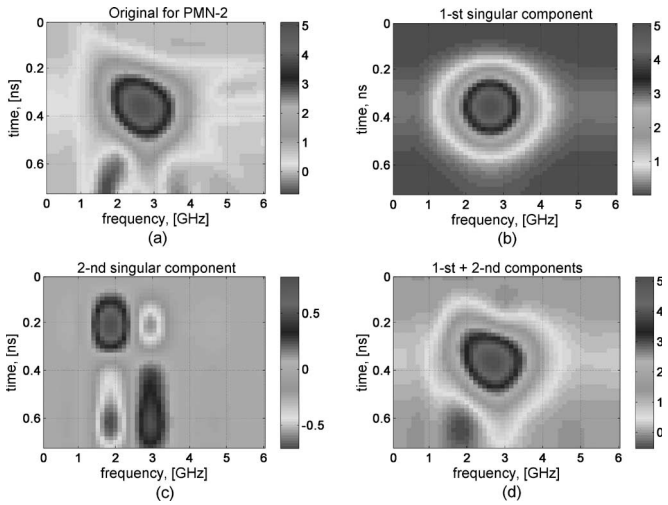

Fig. 5. Approximation of EWD by principal singular components.

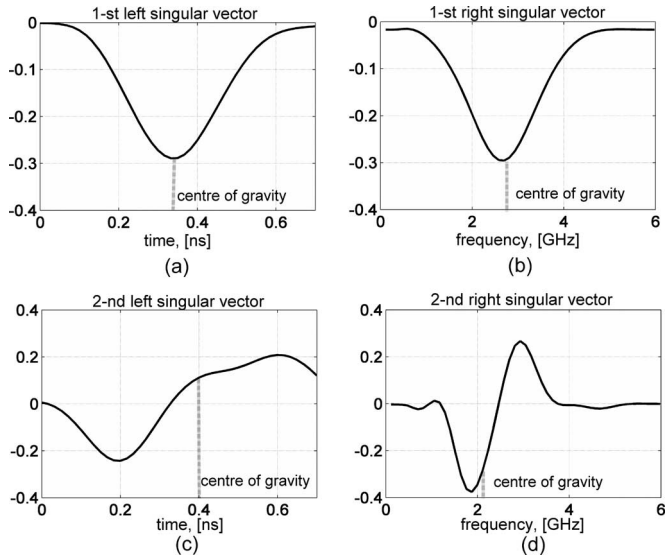

Fig. 6. Feature extraction from singular vectors of EWD.

while the second component (and the others) expresses image details [Fig. 5(c)]. Higher order singular components (the third and higher) can be very discriminant for the EWDs of different targets but lack robustness for the same target, as they significantly change due to any small modification of the EWD or, in other words, due to any change of the target response. Since our purpose is to find stable features, we reject these components as they are nonstationary.

D. Feature Extraction

Singular values of the WD as features for landmine discrimination have been used in a number of works [5], [18], [25], [26], [29]. Their high sensitivity to the target response's energy causes a serious problem for target discrimination at different depths. Besides, an essential target information is contained not only in the singular values but also in the respective singular vectors. Here, we propose to extract target features from both singular values and vectors of the EWD.

Singular vectors are responsible for the shape of the EWD and, as such, they are extremely sensitive to any changes in the target's impulse response shape. The center of gravity of a singular vector represents its integral feature and can be considered as the most robust point. Since the size of the EWD matrix changes with depth, the center should be normalized with respect to the length of the singular vector. Accounting for the unit energy of the singular vectors, the features for the principal EWD components are defined as follows:

$$t_{1,2} = \frac{1}{K}\sum_{k=1}^{K} k\mathbf{u}_{1,2}^2[k]$$
$$f_{1,2} = \frac{1}{L}\sum_{l=1}^{L} l\mathbf{v}_{1,2}^2[l] \tag{8}$$

where K and L are the effective EWD duration and bandwidth, respectively. Fig. 6 illustrates the features of the singular vectors for the EWD given in Fig. 5(a).

The singular values of the principal components are also normalized as follows:

$$\sigma_{1,2\ \mathrm{norm}} = \frac{\sigma_{1,2}}{\|\mathrm{EWD}\|_F} \approx \frac{\sigma_{1,2}}{\sqrt{E}} \tag{9}$$

where $\| \bullet \|_F$ stands for the Frobenius norm of the matrix and E is given by (4). Such normalization makes the singular values nondimensional and invariant to change of energy for the same target.

E. Feature Selection

In total, we extract six parameters from the EWD, namely $t_1, t_2, f_1, f_2, \sigma_{1\ \mathrm{norm}}$, and $\sigma_{2\ \mathrm{norm}}$. These parameters can be used as target features directly, i.e., the target discrimination is to be performed in a six-dimensional feature space. However, we know that for a time-domain signal, its spectrum and time–frequency representation physically contain the same target information. Also, we know that the signal duration and bandwidth are interrelated via the time-bandwidth product. Thus, we may reduce the dimensionality of the feature space by multiplying the parameters t_k and f_k for the same principal component. Finally, we define the following time–frequency features:

$$\begin{aligned}\delta_1 &= t_1 f_1\\ \delta_2 &= t_2 f_2\\ \delta_3 &= \sigma_{1\ \mathrm{norm}}\\ \delta_4 &= \sigma_{2\ \mathrm{norm}}.\end{aligned} \tag{10}$$

The robustness and the discriminant power of the features can be evaluated for a number of GPR scenarios with the same targets. If we think of the target features as coordinates in the 4-D or N-D space, every GPR scenario will be represented by

a point in this feature space. Ideally, we should have a dense cluster of such points for the same target, and such clusters should be separated from each other for different targets.

The separation between two feature clusters expressing mines targets and non-mines targets respectively in N-D space can be estimated with the Mahalanobis distance in (11), shown at the bottom of the page, where symbol $^{\mathrm{T}}$ stands for transpose; $\overline{\boldsymbol{\delta}}_{\mathrm{mines}} = (1/M)\sum_{m=1}^{M} \boldsymbol{\delta}_{\mathrm{mines}}[m]$ is the mean feature vector for the cluster of the mines; $\boldsymbol{\delta}^{\mathrm{T}}_{\mathrm{mines}}[m] = |\delta_1^{\mathrm{mines}}[m] \;\; \delta_2^{\mathrm{mines}}[m] \;\; \cdots \;\; \delta_N^{\mathrm{mines}}[m]|$ is the feature vector for the mth GPR scenario; M is the number of GPR scenarios, N is the number of features; $\boldsymbol{\Lambda}_{\mathrm{mines}} = (1/(M-1))\sum_{m=1}^{M} \boldsymbol{\delta}_{\mathrm{mines}}[m] \cdot \boldsymbol{\delta}^{\mathrm{T}}_{\mathrm{mines}}[m]$ is the covariance matrix for the feature vectors of the mines; $\overline{\boldsymbol{\delta}}_{\mathrm{non-mines}}$, $\boldsymbol{\Lambda}_{\mathrm{non-mines}}$, and $\boldsymbol{\delta}_{\mathrm{non-mines}}[m]$ have the same definition but for the non-mines. For every cluster, the mean feature vector defines its center and the covariance feature matrix defines its size. The cluster itself is approximated by an ellipsoid.

Using the Mahalanobis distance, we can compare the discriminant power of the features (10) with that of the original six features of the principal EWD components. Furthermore, it makes sense to reduce the number of features to a 3-D case by omitting $\sigma_{2\ \mathrm{norm}}$ in order to visualize the feature clusters, i.e., to show the possibility of landmine discrimination in the most explicit way.

III. Experimental Analysis of Feature Clusters

A. Data Acquisition and Preprocessing

Laboratory experiments have been carried out at the Tohoku University, Japan. Our targets were mock mines PMN-2 and Type 72, a stone with size similar to the PMN-2 and a plastic foam model of the Type 72 mine. We intentionally chose the non-mines resembling the mines in order to test a possibility of their discrimination based on the dielectric properties and inner structure of the targets rather than on the difference in size and shape. The targets are shown in Fig. 7. The dimensions of the mines are 120 × 53 mm for the PMN-2 and 78 × 38 mm for the Type 72. The relative dielectric constant is 2.5–2.9 for the mines, 3.5 for the stone, and 1.2 for the plastic foam. The quantity of metal in the PMN-2 is about 1 g, in the Type 72 approximately 0.4 g.

The GPR system included one transmitting–receiving pair of the antipodal Vivaldi antennas and a network analyzer with the frequency range 300 kHz–6 GHz (HP8753D). The antenna pair is a key element of the SAR–GPR array designed at the Tohoku University for vehicle use [3]. The antenna characteristics measured in an anechoic chamber are shown in Fig. 8. The antenna passband limits the GPR bandwidth and, in our case, it is 0.3–7 GHz at a level of −20 dB. Therefore, the frequency range

Fig. 7. GPR targets. Plastic foam, stone, PMN-2, and Type 72.

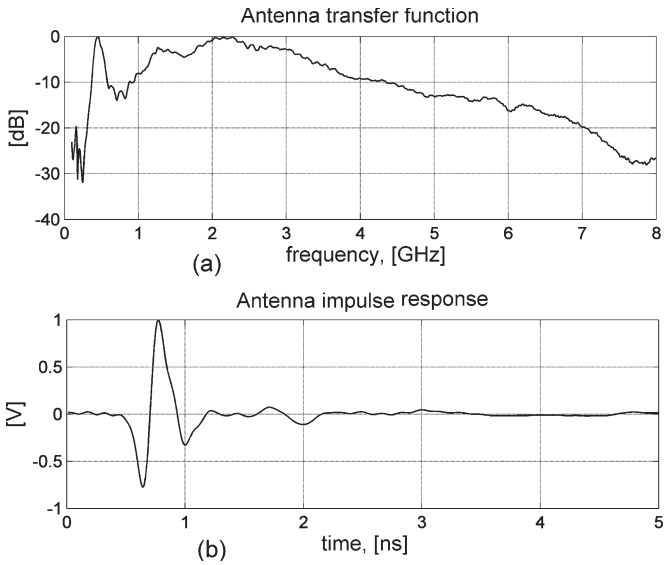

Fig. 8. Vivaldi antenna characteristics.

of the sweep was chosen to be from 0.3 to 6 GHz. The antenna system was fixed on an X-Y translation table.

The antenna height above the ground surface was chosen to be 10 cm. This height is very common in GPR landmine detection as a tradeoff between such factors as the energy attenuation, decreasing the antenna-soil coupling, avoiding possible obstacles of the ground surface, and forming the sufficient antenna footprint for the SAR processing. Besides, the 10 cm provides a near-field zone for the very low radiated frequencies as well as for the high frequencies, concerning the well-known relationship between the antenna aperture and the wavelength $R \geq 2D^2/\lambda$ (far-field condition). The aperture of the Vivaldi antenna is 20 cm, which corresponds to a near-field boundary

$$d = \sqrt{(\overline{\boldsymbol{\delta}}_{\mathrm{mines}} - \overline{\boldsymbol{\delta}}_{\mathrm{non\text{–}mines}})^{\mathrm{T}} (\boldsymbol{\Lambda}_{\mathrm{mines}} + \boldsymbol{\Lambda}_{\mathrm{non\text{–}mines}})^{-1} (\overline{\boldsymbol{\delta}}_{\mathrm{mines}} - \overline{\boldsymbol{\delta}}_{\mathrm{non\text{–}mines}})} \tag{11}$$

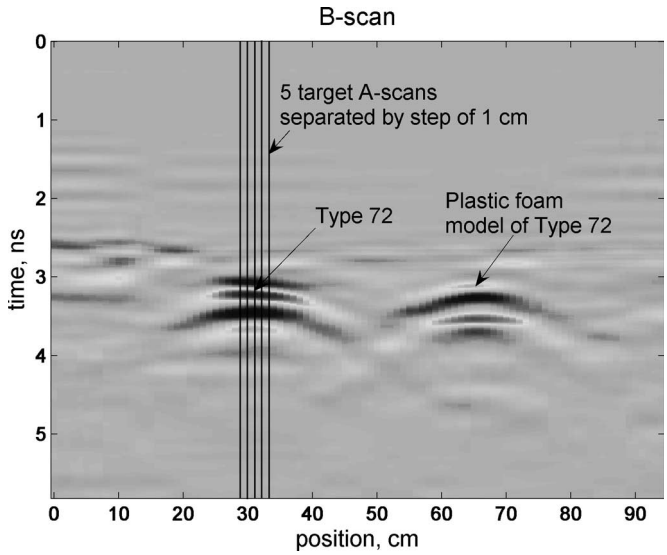

Fig. 9. Selection of target A-scans for feature cluster analysis.

of 8 cm for the 0.3 GHz, 11 cm for the 0.4 GHz, 13 cm for the 0.5 GHz, and etc. Thus, consistency has been obtained for the entire radiated spectrum.

Since the scope of this paper is the feature extraction of the UWB target response, other GPR problems such as roughness of the ground surface and inhomogeneity of soil were minimized. The targets were buried in slightly wet sand with ideally flat surface. Time-domain reflectormeter measurement of the moisture content resulted in 8% from which we estimate a dielectric constant of five. The moisture content corresponds to standard conditions found in minefields in Afghanistan [8]. The burial depth of the targets ranges from 2 to 10 cm with a step of 2 cm. At each depth, a B-scan is acquired over the targets. No targets buried flush or laid on the surface were considered as the ground reflection cannot be removed in this case without strong distortion of the target impulse response.

The preliminary signal processing consists of the subtraction of the antenna crosstalk, acquired beforehand in an anechoic chamber, the IFT with a bandpass filter (left smoothing edge 0.3–1.3 GHz, flat top 1.3–5 GHz, and right smoothing edge 5–6 GHz) and average subtraction clutter removal. Then, the five strongest adjacent A-scans (with a step of 1 cm) were selected from a B-scan target hyperbola, as representative signals. Fig. 9 illustrates the selection of such A-scans. By doing so, we intend to analyze the effect of the horizontal GPR offset from the center of a target on the time–frequency features. Clutter residues in the selected A-scans were suppressed automatically by the time-gating algorithm described in Section II-A.

In summary, for each of the considered targets, five A-scans (corresponding to different GPR horizontal positions above the target) have been acquired, and this for five different burial depths. In total, 25 signals (A-scans) have been obtained for each target. For each of the signals, the EWD has been computed from which we estimated the set of features as defined in Section II-C.

For comparison, a dataset acquired under realistic circumstances was processed. The used sensor is a UWB array of six emitters and six receivers with a bandwidth of 0.5–4.5 GHz (DEMINE) [4]–[6], [31]. The excitation is based on a pseudo-random noise signal. The data were acquired during a field campaign in Angola. The mines were emplaced by experienced deminers in a cleared portion of a minefield. The soil was very dry. Also, the surface of the test lanes was similar to the surface of the minefield, i.e., rough and cluttered with small stones. The mines were buried several weeks before the tests took place, so the mines and the surrounding ground were given sufficient time to settle. Therefore, we can consider these as realistic test circumstances.

Out of the data, four objects are selected, three antipersonnel mines (Type 72, PMA-3 and PPM2) and a Grenade. The Type 72 was buried at a depth of 3 cm. It had its original explosive filling, a surrogate booster charge, and the original detonator. The PMA-3 is a cylindrical mine of diameter 103 mm and height 37 mm, it was buried at a depth of 5 cm. It had a surrogate explosive filling and a surrogate detonator. The PPM2 is also a cylindrical with a diameter of 124 mm and a height of 63 mm, its burial depth was 12 cm. It had a surrogate explosive filling and a surrogate detonator. The Grenade resembles a cylinder of length 300 mm and diameter of 100 mm. It was a shaped-charge stick grenade without detonator or handle, with its original explosive filling, buried at a depth of 8 cm. The burial depths are known approximately due to the roughness of the soil. The surrogate explosive is a two-part rubber molding formula called RTV 3110. This is a casting rubber that has a dielectric constant, thermal conductivity, density and radar image that mimics TNT very closely.

The data were preprocessed with a source-signal deconvolution, antenna crosstalk subtraction, adaptive clutter removal [32], and with automatic time gating. The adaptive clutter removal consists of taking a background A-scan (no object present) and time shifting, and scaling it so the ground reflection coincides with that of the measured signal before subtracting. This method lessens the distortion of overlapping signals between the mine and the air–ground interface. Then, for each object, ten A-scans were selected in a square area of 15 cm above the objects.

Concerning the computational expenses, it takes 0.91 s on a laptop with 1.7-GHz Pentium M processor and 512-MB memory to preprocess one B-scan (matrix 512×131) by antenna crosstalk subtraction, transformation into the time domain and average subtraction, to extract a target's impulse response (512-element vector), to compute the EWD, and to extract the full set of six features. The total processing time for the four targets and the 25 signals per target was 91 s. The processing was performed in MATLAB ver. 7.01 working under Windows XP Professional.

B. Feature Clustering and Discriminant Power

For the laboratory data, we first analyze the reduced set of 3-D features δ_1, δ_2, and δ_3 defined by (10). They are depicted in Fig. 10 for each of the considered targets and for the 25 signals per target. As it can be seen, the estimated features for every target can be divided into two separated clusters: the first cluster represents the depth of 2 cm while the second includes all the other depths. Therefore, we can conclude that

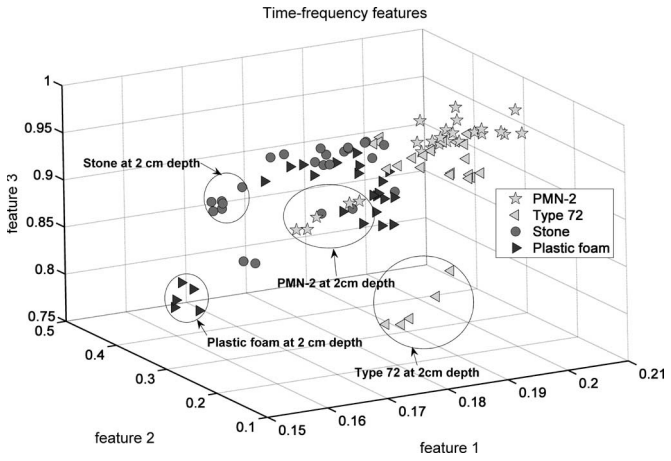

Fig. 10. Features extracted from both singular values and vectors of EWD for depths 2–10 cm.

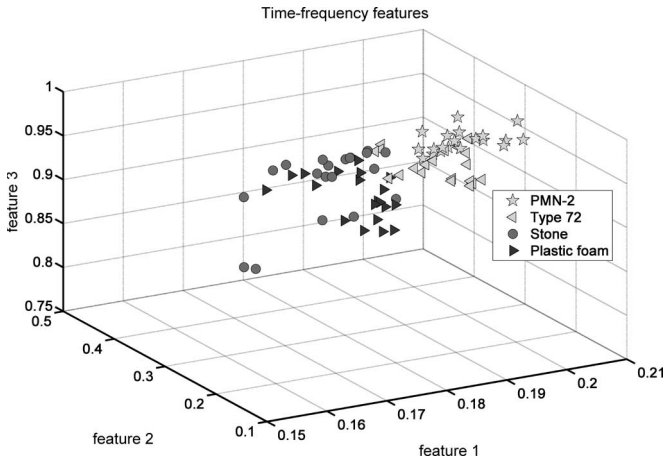

Fig. 11. Features extracted from both singular values and vectors of EWD for depths 4–10 cm.

at very shallow depths, the time–frequency features are very different from those of deeper targets. The most important reason for this is the strong distortion of the target response by the ground interface. The second reason is that the soil's layer above such a shallow target influences its response much less than for larger depths. However, all the targets at 2 cm are well separated from each other, which means that the time–frequency discrimination for very small and larger depths should be performed separately, i.e., two feature libraries, created respectively for the depths, less than 3 cm and deeper, are necessary to discriminate the same landmine.

Fig. 11 shows the features for the depths 4, 6, 8, and 10 cm. One can notice a good separation between the mines and the non-mines in the considered feature space. However, the PMN-2 cannot be discriminated from the Type 72 in spite of their significant difference in size, since their features form one good cluster. Both landmines are well discriminated from the stone and the plastic foam. The latter targets resemble the landmines in size and shape but have different dielectric constant. This means that the proposed features are implicitly related to the dielectric constant. For comparison, Fig. 12 shows the first three singular values of the EWD normalized according

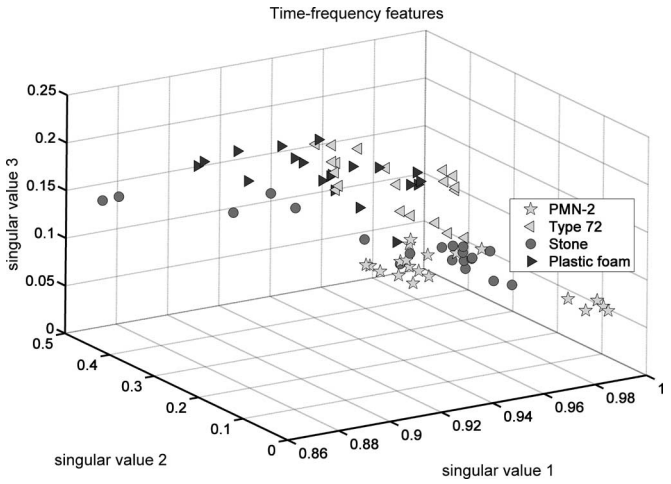

Fig. 12. Features extracted from singular values of EWD.

to (9). Here, the landmines cannot be distinguished from the other objects at all. Thus, the features given by (10) provide good discriminant information about the targets.

The next step is to compare numerically the discriminant power or separability of different feature vectors. This is done using the Mahalanobis distance between the cluster of landmines and the cluster of non-mines as defined in (11). Since the features are normalized, the Mahalanobis distance values can be directly compared. Next to the Mahalanobis distance, Wilk's lambda (WL) discriminant analysis has also been used [26]. The WL value expresses how well feature vectors belonging to one class are clustered together, taking into account the between and the within class distances. The WL values are always between zero and one; with zero, meaning perfect class separation, and one, no class separation. Table I summarizes the criteria values estimated for several feature sets. Two classes are considered, the mine and non-mine objects, respectively. Then, in each class, the number of GPR scenarios M in (11) is defined as two targets multiplied by four different depths and by five different A-scans which results in 40 scenarios (feature vectors). Case 1 gives the values for each feature separately, showing that none of the separate features is well discriminant, maybe except for f_1 which is the most discriminant feature. Cases 2 and 3 show the results of combining the first and the second groups of features. There is a significant improvement, but the results are not yet satisfying. Case 4 represents the 3-D features visualized in Fig. 11, while Case 4 is for the 4-D features defined by (10). Cases 6 and 7 show the results for the five features and the full set of six features, respectively. Case 7 provides the best discriminant power for the two different criteria.

Finally, Fig. 13 shows the results for the DEMINE data. The plastic landmines (Type 72, PMA-3, and PPM2) are well separated from the metal grenade. Here, in addition to the difference in dielectric properties and inner structure, a considerable difference in size of the targets is present that results in a good feature separation between the smaller Type 72 and PMA-3, and the larger Grenade and PPM2. Although this dataset was not acquired specifically for the purpose of feature comparison, and thus, no data are available for the same objects at different depths (which is why we omit the numerical

TABLE I
FEATURE DISCRIMINANT POWER

Case	Features	Mahalanobis Distance	Wilk's Lambda
1	$t_1 - f_1 - \sigma_{1norm} - t_2 - f_2 - \sigma_{2norm}$	0.4365 – 1.8214 – 0.5003 – 0.3844 – 0.2434 –0.4962	0.6348 – 0.3665 – 0.5825 – 0.7560 – 0.4106 – 0.6477
2	t_1, f_1, σ_{1norm}	2.1085	0.1936
3	t_2, f_2, σ_{2norm}	1.1566	0.2281
4	$t_1 f_1,\ t_2 f_2,\ \sigma_{1norm}$	2.0769	0.0963
5	$t_1 f_1,\ t_2 f_2,\ \sigma_{1norm}, \sigma_{2norm}$	2.1732	0.0925
6	$t_1, f_1, \sigma_{1norm}, t_2, f_2$	2.2530	0.0890
7	$t_1, f_1, \sigma_{1norm}, t_2, f_2, \sigma_{2norm}$	2.2892	0.0796

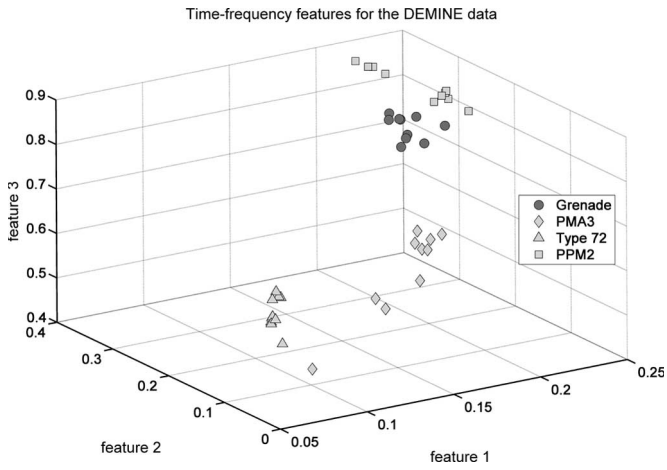

Fig. 13. Features for DEMINE GPR.

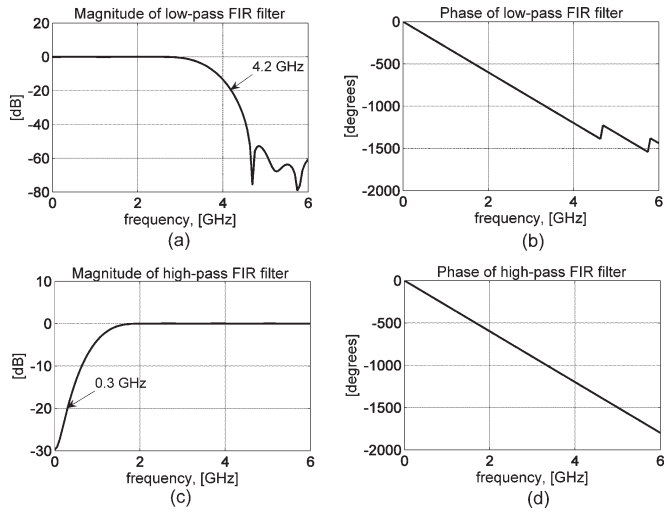

Fig. 14. FIR filters.

criteria-based features evaluation here), the clear separation of targets, the method shows under very different conditions (different sensor and realistic conditions), indicates its robustness.

C. Feature Dependence on GPR Bandwidth

The targets impulse responses have been acquired in a large frequency range, specifically 0.3–6 GHz. By high- and low-pass filtering the targets' impulse responses, the feature separability dependence on frequency range has been evaluated as well as the informative properties of the low and high frequencies. Here, we analyzed the targets at the depths of 4–10 cm, i.e., 20 A-scans per target forming one feature cluster. Since the data preprocessing to obtain the targets' impulse responses was linear, such evaluation can directly be used to determine the optimal GPR bandwidth providing the maximal features separability for the given targets and the soil. The cutoff frequency of a low-pass (high-pass) filter at the -20 dB corresponds to the higher (lower) frequency of the GPR with a smaller bandwidth. The finite-impulse-response (FIR) filters were used due to their linear phase characteristic. The FIR filters have been designed by means of the signal processing toolbox in MATLAB. As example, low-pass and high-pass FIR filters, used in the further processing, are shown in Fig. 14.

Fig. 15 depicts the results of the low-pass filtering for the PMN-2 buried at a depth of 6 cm. The filtering was performed in the forward and backward directions to compensate for the phase shift. The signals in Fig. 15(a) do not look very different in spite of their different spectra in Fig. 15(b). Meanwhile, the time–frequency representations before and after filtering differ from each other significantly, as shown in Fig. 15(c) and (d). Besides the changed image of itself, the effective bandwidth is reduced while the effective duration is increased. This result illustrates the high sensitivity of the EWD to the GPR bandwidth. If we reduce the latter step by step and estimate the features separability; then, we can find which frequencies are informative and which are not.

The Mahalanobis distance as a function of the GPR higher and lower frequencies has been chosen as a criterion for optimality. At first, we evaluated the influence of low frequencies. In order to do this, the original targets' impulse responses were filtered with a high-pass FIR filter. The filter cutoff frequency, considered as the GPR lower frequency, was gradually

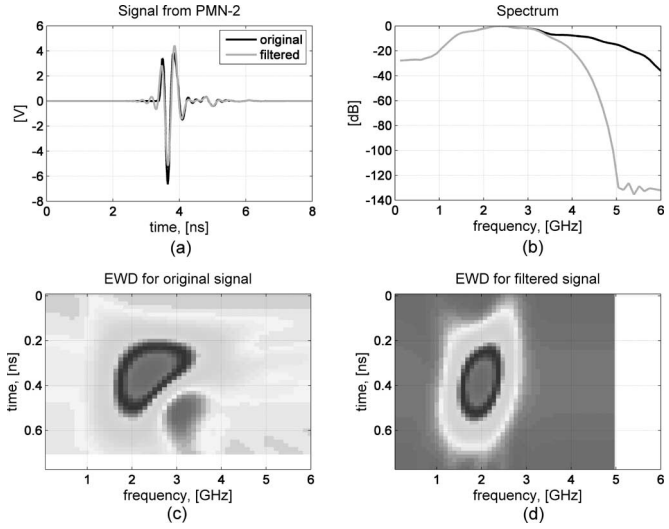

Fig. 15. Influence of data bandwidth on EWD.

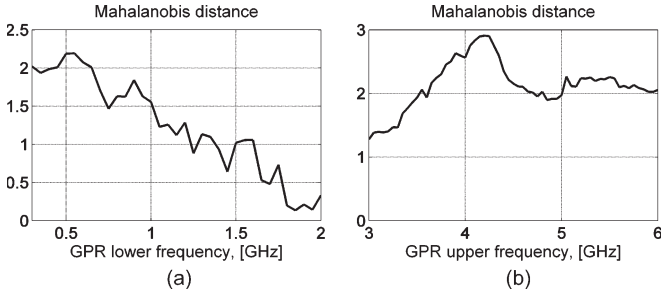

Fig. 16. Frequency dependence of features separability.

increasing from 0.3 to 2 GHz with a step of 50 MHz. At each step, the targets' impulse responses were filtered, the 3-D feature clusters were extracted (Case 4 in Table I), and the Mahalanobis distance between the mines as one class and the stone as another class was computed. Here, we excluded the plastic foam as its dielectric constant is very different from that of the stone, and therefore, its features depend on the GPR bandwidth in a different way. The result is depicted in Fig. 16(a). The Mahalanobis distance dependence does not reveal a strong maximum and decreases with the frequency. Thus, the low-frequency information is very important for the time–frequency discrimination, and the GPR lower frequency must be as low as possible.

Then, starting from the original data, the influence of high frequencies has been evaluated with a low-pass FIR filter. Its cutoff frequency, considered as the GPR upper frequency, was decreasing from 6 to 3 GHz with the step of 50 MHz. The Mahalanobis distance dependence has a clear maximum at 4.2 GHz, as shown in Fig. 16(b). Thus, 4.2 GHz is the optimal GPR upper frequency providing the best feature separability, while the higher frequencies can be considered as not informative for the selected targets and the soil.

In order to validate the obtained results, we visualize the features for the optimal and nonoptimal GPR bandwidth. Fig. 17 shows the features extracted from the filtered data with the upper frequency of 4.2 GHz. Compared to Fig. 11, the landmines are noticeably better separated from the stone. Meanwhile, the data with the upper frequency of 3 GHz do not allow

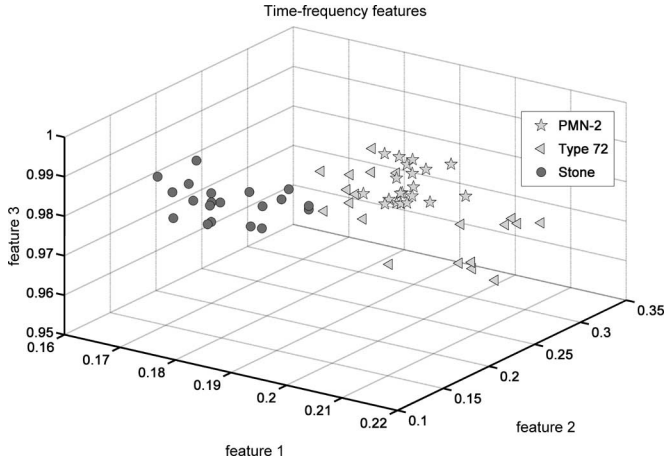

Fig. 17. Features for GPR bandwidth of 0.3–4.2 GHz.

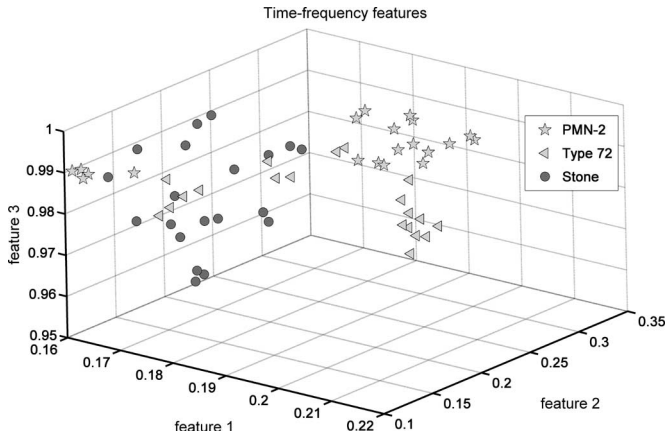

Fig. 18. Features for GPR bandwidth of 0.3–3 GHz.

discrimination at all, as illustrated in Fig. 18. This indicates that the essential target information exists above 3 GHz as well.

IV. Discussion and Conclusion

Our results demonstrate the possibility for automatic target discrimination following the stage of GPR target detection. For that, a few time–frequency features can be extracted from the early-time target impulse response and then classified on the basis of a features library, which has been constructed beforehand. Numerically, the proposed feature extraction is inexpensive. The computation needed to extract the target impulse response from a raw B-scan (512×131) and its time–frequency features takes 0.91 s on an average computer. The effectiveness of target discrimination depends on both the GPR hardware and the complete signal-processing software, which must include algorithms of target detection, clutter removal, feature extraction, and feature classification. In this paper, we focused only on the feature extraction and investigated the time–frequency features of a nonstationary target response in fully controlled laboratory conditions. The data were acquired with a stepped-frequency GPR for the frequency range of 0.3–6 GHz. The soil was sand with a moisture content of 8%.

Discriminant target features have been proposed, using both the singular values and the singular vectors of the EWD

considered as a time–frequency target image. For the feature robustness, only the first two singular triplets were used as the principal components. In total, the target impulse response can be characterized by six features normalized accordingly by the effective signal duration, the effective bandwidth, and the energy. Multiplication of the time and frequency features of the respective singular vectors reduces the feature space to the 3-D case without a significant loss of discriminant power and makes the visual analysis of the feature clusters possible. To evaluate the discriminant power, two different criteria, namely the Mahalanobis distance between the feature clusters and WL, are used.

The features allow the discrimination between landmines (the PMN-2 and Type 72 in our case) and landminelike dielectric targets in the range of depths 2–10 cm and for different GPR positions above the target. An A-scan corresponding to the target's edge can be used for the discrimination as well as an A-scan above the target's center. Another important conclusion is that the time–frequency approach does not work simultaneously for a very shallow target, buried at 2 cm or less, and the same target buried deeper due to distortion by the air–ground interface and influence of the soil. Thus, very shallow targets as well as targets buried flush or laid on the surface should be processed with a features library created specifically for such conditions, while deeper targets should employ a separate features library.

Using the proposed features, we could not distinguish between the two landmines, in spite of significant difference in size, so they should be considered as one target class. However, both landmines were well discriminated from the stone with a size similar to the PMN-2, and from a plastic foam model of the Type 72 mine. Thus, we can assume that the time–frequency features are implicitly related to the dielectric constant of the targets.

The feature dependence on the low and high frequencies of the target's response has been analyzed in the frequency range of 0.3–6 GHz. The low frequencies were found to be very important for the landmine discrimination. This imposes a requirement on the GPR lower frequency to be as low as possible. Meanwhile, it has been shown that the frequency range of 0.3–4.2 GHz at a -20-dB level provides the best feature separability between the landmines and the stone. Hence, the optimal GPR upper frequency for the given soil is 4.2 GHz. These results are an important hint for developers of GPR hardware.

The frequency behavior of the features allows us to estimate in what kind of soil the time–frequency landmine discrimination can be effective. Obviously, a lossy soil strongly attenuates high frequencies of the GPR sensing signal. If a target's response has its frequencies below 4.2 GHz suppressed by soil, then the developed feature extraction is less robust. A study of practical interest can be carried out in this direction with a purpose to establish a relationship between the attenuation of such frequencies for a standard target and the moisture content measured in the field.

The features proposed have been tested on a realistic dataset acquired with a pseudonoise GPR DEMINE in Angola and showed a good discrimination power.

REFERENCES

[1] M. Sato, Y. Hamada, X. Feng, F. N. Kong, Z. Zeng, and G. Fang, "GPR using an array antenna for landmine detection," *Near Surface Geophys.*, vol. 2, no. 1, pp. 5–11, Feb. 2004.

[2] X. Feng and M. Sato, "Pre-stack migration applied to GPR for landmine detection," *Inverse Probl.*, vol. 20, no. 6, pp. 1–17, Dec. 2004.

[3] M. Sato, X. Feng, T. Kobayashi, Z. Zhou, T. G. Savelyev, and J. Fujiwara, "Development of an array-antenna GPR system (SAR-GPR)," in *Proc. SPIE—Detection and Remediation Technologies for Mines and Minelike Targets X*, 2005, vol. 5794, pp. 480–487.

[4] D. J. Evans and S. R. Cloude, "An ultra-wideband antenna array for ground penetrating radar mine detection," in *Proc. AP2000*, Davos, Switzerland, 2000, pp. 1–4.

[5] DEMINE partners. Public Report D16, *European Project 29902 DEMINE*, 2002. [Online]. Available: http://www.eudem.vub.ac.be/files/demine_final_report.pdf

[6] J. Sachs, "M-sequence radar," in *Ground Penetrating Radar*, 2nd ed. ser. IEE Radar, Sonar, Navigation and Avionics Series 15, D. J. Daniels, Ed. London, U.K.: Inst. Electr. Eng., 2004, pp. 225–237.

[7] M. Sato, J. Fujiwara, X. Feng, Z. Zhou, and T. Kobayashi, "Development of a hand-held GPR MD sensor system (ALIS)," in *Proc. SPIE—Detection and Remediation Technologies for Mines and Minelike Targets X*, vol. 5794, pp. 1000–1007.

[8] M. Sato, X. Feng, T. Kobayashi, Z. Zhou, T. G. Savelyev, and J. Fujiwara, "Preparation of GPR+MD sensors evaluation tests in Japan and Afghanistan," in *Proc. SPIE—Detection and Remediation Technologies for Mines and Minelike Targets X*, 2005, vol. 5794, pp. 919–928.

[9] K. C. Ho, L. M. Collins, L. G. Huettel, and P. D. Gader, "Discrimination mode processing for EMI and GPR sensors for hand-held land mine detection," *IEEE Trans. Geosci. Remote Sens.*, vol. 42, no. 1, pp. 249–263, Jan. 2004.

[10] P. D. Gader, M. Mystkowski, and Y. Zhao, "Landmine detection with ground penetrating radar using hidden Markov models," *IEEE Trans. Geosci. Remote Sens.*, vol. 39, no. 6, pp. 1231–1244, Jun. 2001.

[11] Q. Zhou and L. M. Collins, "Application of feature extraction methods for landmine detection using the Wichmann/Niitek ground penetrating radar," *IEEE Trans. Geosci. Remote Sens.*, vol. 43, no. 1, pp. 81–85, Jan. 2005.

[12] L. Y. Astanin and A. A. Kostylev, *Ultra-Wideband Radar Measurements: Analysis and Processing*, ser. IEE Radar, Sonar, Navigation and Avionics Series 7. London, U.K.: Inst. Electr. Eng., 1997.

[13] F. Roth, "Convolutional models for landmine identification with ground penetrating radar," Ph.D. dissertation, Delft Univ. Technol., Delft, The Netherlands, 2005.

[14] A. van der Merwe and I. J. Gupta, "A novel signal processing technique for clutter reduction in GPR measurements of small, shallow land mines," *IEEE Trans. Geosci. Remote Sens.*, vol. 38, no. 6, pp. 2627–2637, Nov. 2000.

[15] A. M. Zoubir, I. J. Chant, C. L. Brown, B. Barkat, and C. Abeynayake, "Signal processing techniques for landmine detection using impulse ground penetrating radar," *IEEE Sensors J.*, vol. 2, no. 1, pp. 41–51, Feb. 2002.

[16] T. G. Savelyev, L. van Kempen, and H. Sahli, "Deconvolution techniques," in *Ground Penetrating Radar*, 2nd ed. ser. IEE Radar, Sonar, Navigation and Avionics Series 15, D. J. Daniels, Ed. London, U.K.: Inst. Electr. Eng., 2004, pp. 298–310.

[17] T. G. Savelyev and M. Sato, "Comparative analysis of UWB deconvolution and feature extraction algorithms for GPR landmine detection," in *Proc. SPIE—Detection and Remediation Technologies for Mines and Minelike Targets IX*, 2004, vol. 5415, pp. 1008–1018.

[18] T. G. Savelyev, L. van Kempen, and H. Sahli, "GPR anti-personnel landmine detection: Improved deconvolution and time-frequency feature extraction," in *Proc. SPIE—Nondestructive Evaluation and Health Monitoring of Aerospace Materials and Composites II*, 2003, vol. 5046, pp. 232–241.

[19] T. G. Savelyev and M. Sato, "UWB GPR target identification for landmine detection," in *Proc. 7th Int. Symp. Soc. Exploration Geophysicists Jpn.—Imaging Technology*, 2004, pp. 124–129.

[20] ——, "Optimal GPR bandwidth for time-frequency landmine discrimination," in *Proc. SPIE—Detection and Remediation Technologies for Mines and Minelike Targets X*, 2005, vol. 5794, pp. 435–446.

[21] H. Strifors, B. Brusmark, A. Gustaffson, and G. Gaunaurd, "Analysis in the joint time-frequency domain of signatures extracted from targets buried underground," in *Proc. SPIE—Automatic Object Recognition VI*, 1996, vol. 2756, pp. 152–163.

[22] G. Gaunaurd and H. Strifors, "Applications of time-frequency signature analysis to target identification," in *Proc. SPIE—Wavelet Applications VI*, 1999, vol. 3723, pp. 78–90.

[23] H. C. Strifors, G. C. Gaunaurd, and A. J. Sullyvan, "Simultaneous classification of underground targets and determination of burial depth and soil moisture content," in *Proc. SPIE—Automatic Target Recognition XIV*, 2004, vol. 5426, pp. 256–263.
[24] F. Roth, P. van Genderen, and M. Verhaegen, "Analysis of the influence of mine and soil properties on features extracted from GPR data," in *Proc. SPIE—Detection and Remediation Technologies for Mines and Minelike Targets VI*, 2001, vol. 4394, pp. 428–439.
[25] Y. Sun and J. Li, "Plastic landmine detection using time-frequency analysis for forward-looking ground penetrating radar," in *Proc. SPIE—Detection and Remediation Technologies for Mines and Minelike Targets VIII*, 2003, vol. 5089, pp. 851–862.
[26] L. van Kempen, H. Sahli, E. Nyssen, and J. Cornelis, "Signal processing and pattern recognition methods for radar AP mine detection and identification," in *Proc. Inst. Electr. Eng. 2nd Int. Conf. Detection Abandoned Landmines*, Edinburgh, U.K., 1998, vol. 458, pp. 81–85.
[27] M. Fritzsche, "Detection of buried landmines with GPR," in *Ground Penetrating Radar*, 2nd ed. ser. IEE Radar, Sonar, Navigation and Avionics Series 15, D. J. Daniels, Ed. London, U.K.: Inst. Electr. Eng., 2004, pp. 540–557.
[28] S. Qian and D. Chen, *Joint Time-Frequency Analysis: Methods and Applications*. Englewood Cliffs, NJ: Prentice-Hall PTR, 1996.
[29] H. Brunzell, "Signal processing techniques for detection of buried landmines using ground penetrating radar," Ph.D. dissertation, Dept. Signals Syst., Chalmers Univ. Technol., Geterborg, Sweden, 1998.
[30] G. Golub and C. V. Loan, *Matrix Computations*. Baltimore, MD: John Hopkins Univ. Press, 1989.
[31] J. A. Ratcliffe, J. Sachs, S. Cloude, G. N. Crisp, H. Sahli, P. Peyerl, and G. De Pasquale, "Cost effective surface penetrating radar device for humanitarian demining," in *Ultra-Wideband, Short-Pulse Electromagnetics 5*, P. D. Smith and S. R. Cloude, Eds. New York: Plenum, 2002, pp. 275–283.
[32] J. Brooks, L. van Kempen, and H. Sahli, "Ground penetrating radar data processing: Clutter characterization and removal," ETRO Dept., Vrije Univ. Brussel, Brussels, Belgium, Tech. Rep. IRIS-TR-0059, 1999.

Timofey Grigorievich Savelyev was born in Frunze, Soviet Union, in 1974. He received the Dipl.-Eng. (*cum laude*) degree in radio electronics from the Baltic State Technical University, St. Petersburg, Russia, in 1997 and the Ph.D. degree in electrical engineering, for his research in adaptive array radar systems, from the State University of Aerospace Instrumentation, St. Petersburg, in 2000.

Since then, he worked in the field of GPR landmine detection as a Visiting Scientist with Vrije Universiteit Brussel, Brussels, Belgium, in 2002, then, as a Research Associate with the Center for Northeast Asian Studies, Tohoku University, Sendai, Japan, from 2003 to 2005. Currently, he is a Postdoctoral Researcher with the International Research Centre for Telecommunications and Radar, Delft University of Technology, Delft, The Netherlands. His current research interests include GPR landmine detection, UWB array radars, UWB signal processing and analysis, and radar imaging.

Luc van Kempen was born in Vilvoorde, Belgium, in 1971. He received the Masters degree in electrical engineering from Vrije Universiteit Brussel (VUB), Brussels, Belgium, in 1995 and the Ph.D. degree in engineering sciences on the topic of the detection of antipersonnel landmines using GPR from VUB.

He had specialized in biomedical engineering techniques and then joined the Department of Electronics and Information Processing, VUB. His research interests include radar imaging, electromagnetics, tomography, and subsurface sensing.

Hichem Sahli (A'00–M'03) was born in Tunis, Tunisia, in 1960. He received the Ph.D. degree in computer sciences from the Ecole Nationale Supérieure de Physique Strasbourg, Strasbourg, France, in 1991.

He is currently a Professor of image processing and computer vision with the Department of Electronics and Informatics, Vrije Universiteit Brussel, Brussels, Belgium. He coordinates two research teams on computer vision and landmine detection. His research is focused on two broad areas, namely, inverse problems in vision, models for vision and the development of algorithms for scene interpretation. The work conducted by his research team is motivated by applications in the fields of imaging, computer vision, and autonomous navigation.

Juergen Sachs received the Dipl.-Ing. degree in semiconductor physics and technology and the Dr.-Ing. degree for his research in the field of surface acoustic wave devices, both from the Technical University of Ilmenau, Germany, in 1975 and 1980, respectively.

From 1982 to 1985, he was a Senior Lecturer with the National Institute of Electronics Sétif, Algeria. Since 1985, he has been a Senior Lecturer with the Technical University of Ilmenau, Germany. His lectures cover the basics of electrical measurements, RF-measurement technique, and radar technology. Since 1996, he has been engaged in the research of ultrawideband (UWB) radar. He is the Head of a research group which deals with a wide range of different aspects of UWB technology. This covers the design of new system conceptions, the development of integrated hardware components, as well as research on different applications fields which extend from nondestructive testing to medical engineering. He is a Coordinator of several European research projects joining companies and research institutions from different European countries. He has published quite a few of conference and journal papers and has contributed to several books.

Motoyuki Sato (S'79–M'80–SM'02) received the B.E., M.E., and Dr.Eng. degrees in information engineering in 1980, 1982, and 1985, respectively, all from Tohoku University, Sendai, Japan.

He is currently a Professor with the Center for Northeast Asian Studies, Tohoku University. In 1985, he joined the Faculty of Engineering, Tohoku University. From 1988 to 1989, he was a Visiting Researcher with the Federal Institute for Geoscience and Natural Resources (BGR) in Hannover, Germany. His current research interests include transient electromagnetics and antennas, radar polarimetry, GPR, landmine detection, borehole radar, electromagnetic logging, interferometric and polarimetric SAR.

Dr. Sato has served as a Technical Chairman of the 6th International Conference on Ground Penetrating Radar (GPR'96). He was awarded the Institute of Electronics, Information, Communication Engineers Young Engineer's Award in 1984, the Society of Petrophysicists and Well Log Analysts best Poster Award in 1994, and the Society of Exploration Geophysicists of Japan Best Paper Award in 1999. He is a Chair of the IEEE-GRSS Japan Chapter for 2006 to 2007 and IEEE-GRSS AdCom member for 2006 to 2007.